University Library

MINERVA ACCESS

A gateway to Melbourne's research publications

Minerva Access is the Institutional Repository of The University of Melbourne

Author/s:
Namvar, A;Blanch, AJ;Dixon, MW;Carmo, OMS;Liu, B;Tiash, S;Looker, O;Andrew, D;Chan, LJ;Tham, WH;Lee, PVS;Rajagopal, V;Tilley, L

Title:
Surface area-to-volume ratio, not cellular viscoelasticity, is the major determinant of red blood cell traversal through small channels

Date:
2021-01-01

Citation:
Namvar, A., Blanch, A. J., Dixon, M. W., Carmo, O. M. S., Liu, B., Tiash, S., Looker, O., Andrew, D., Chan, L. J., Tham, W. H., Lee, P. V. S., Rajagopal, V. & Tilley, L. (2021). Surface area-to-volume ratio, not cellular viscoelasticity, is the major determinant of red blood cell traversal through small channels. Cellular Microbiology, 23 (1), https://doi.org/10.1111/cmi.13270.

Persistent Link:
https://hdl.handle.net/11343/252585

License:
CC BY-NC

Received: 29 April 2020 | Revised: 14 August 2020 | Accepted: 18 September 2020

DOI: 10.1111/cmi.13270

Check for updates

WILEY

RESEARCH ARTICLE

# Surface area-to-volume ratio, not cellular viscoelasticity, is the major determinant of red blood cell traversal through small channels

Arman Namvar[1,2] | Adam J. Blanch[1] | Matthew W. Dixon[1] | Olivia M. S. Carmo[1] | Boyin Liu[1] | Snigdha Tiash[1] | Oliver Looker[1] | Dean Andrew[1] | Li-Jin Chan[3,4] | Wai-Hong Tham[3,4] | Peter V. S. Lee[2] | Vijay Rajagopal[2] | Leann Tilley[1]

[1]Department of Biochemistry and Molecular Biology, Bio21 Institute, University of Melbourne, Parkville, Victoria, Australia

[2]Department of Biomedical Engineering, University of Melbourne, Parkville, Victoria, Australia

[3]Division of Infection & Immunity, Walter & Eliza Hall Institute, Parkville, Victoria, Australia

[4]Department of Medical Biology, University of Melbourne, Parkville, Victoria, Australia

**Correspondence**
Leann Tilley, Department of Biochemistry and Molecular Biology, Bio21 Molecular Science and Biotechnology Institute, Melbourne, VIC 3010, Australia.
Email: ltilley@unimelb.edu.au

Vijay Rajagopal, Department of Biomedical Engineering, University of Melbourne, VIC 3010, Australia.
Email: vijay.rajagopal@unimelb.edu.au

**Funding information**
Australian Research Council, Grant/Award Number: FL150100106

## Abstract

The remarkable deformability of red blood cells (RBCs) depends on the viscoelasticity of the plasma membrane and cell contents and the surface area to volume (SA:V) ratio; however, it remains unclear which of these factors is the key determinant for passage through small capillaries. We used a microfluidic device to examine the traversal of normal, stiffened, swollen, parasitised and immature RBCs. We show that dramatic stiffening of RBCs had no measurable effect on their ability to traverse small channels. By contrast, a moderate decrease in the SA:V ratio had a marked effect on the equivalent cylinder diameter that is traversable by RBCs of similar cellular viscoelasticity. We developed a finite element model that provides a coherent rationale for the experimental observations, based on the nonlinear mechanical behaviour of the RBC membrane skeleton. We conclude that the SA:V ratio should be given more prominence in studies of RBC pathologies.

**KEYWORDS**

deformability, plasmodium, red blood cell, reticulocyte, surface area-to-volume ratio

## 1 | INTRODUCTION

The human red blood cell (RBC) comprises a plasma membrane enclosing a concentrated solution (~10 mM) of protein, mainly haemoglobin. The mature RBC (resting long diameter ~8 μm) exhibits remarkable deformability and durability. During its four-month lifespan, a human RBC circulates the body about a million times (Allison, 1960). It undertakes this journey of about 500 hundred kilometres, without repair, squeezing through cerebral capillaries with diameters as small as 3 μm and inter-endothelial slits in the spleen with widths of 1–2 μm (An & Mohandas, 2008; Lauwers, Cassot, Lauwers-Cances, Puwanarajah, & Duvernoy, 2008; Marin-Padilla,- 2012). The ability to undergo large deformations and to conform to narrow shapes is essential for RBC function.

The deformability of RBCs is determined by contributions from the plasma membrane viscoelasticity, the cytoplasmic viscosity and the cellular geometry (Diez-Silva, Dao, Han, Lim, & Suresh, 2010; Mohandas & Gallagher, 2008; Pivkin et al., 2016). The viscoelastic properties of the RBC membrane are in turn determined by a sub-membranous protein meshwork (Mohandas & Gallagher, 2008; Zhang et al., 2015). The

This is an open access article under the terms of the Creative Commons Attribution-NonCommercial License, which permits use, distribution and reproduction in any medium, provided the original work is properly cited and is not used for commercial purposes.
© 2020 The Authors. *Cellular Microbiology* published by John Wiley & Sons Ltd.

membrane skeleton comprises an array of flexible cross-members (spectrin) linked into junctional complexes (actin and accessory proteins; Mankelow, Satchwell, & Burton, 2012). The spectrin molecules act like molecular springs, accommodating the distortions imposed by shear forces in the circulation. Vertical interactions connect the skeletal meshwork to the proteins embedded in the plasma membrane. The cytoplasmic viscosity is dependent on the concentration and physical state of haemoglobin, which may be altered by changes in the hydration level or in some haemoglobinopathies (Kuhn et al., 2017; Renoux et al., 2019). A resting RBC adopts a biconcave discoid shape with a surface area to volume (SA:V) ratio ~1.5-fold greater than a sphere of the same volume. The surface area of a healthy RBC is kept constant, and any increases in volume decrease the SA:V ratio, which adversely impacts RBC rheology.

Upon infection with a malaria parasite, key biomechanical properties of the RBC are subverted. For example, RBCs infected with mature stage *Plasmodium falciparum* – the species responsible for most malaria-related deaths – exhibit significantly decreased deformability (Glenister, Coppel, Cowman, Mohandas, & Cooke, 2002; Park et al., 2008; Suresh et al., 2005). The intracellular parasite exports proteins that stiffen the RBC membrane (de Koning-Ward, Dixon, Tilley, & Gilson, 2016). *P. falciparum* also exports an adhesin, called *P. falciparum* Erythrocyte Membrane Protein-1, that embeds in the RBC membrane and binds to endothelial cell receptors (Wahlgren, Goel, & Akhouri, 2017). Sequestration of infected RBCs in brain capillaries is associated with impaired blood flow within the deep tissue microcapillary beds (Beare, Harding, Taylor, Lewallen, & Molyneux, 2009; Dondorp, Kager, Vreeken, & White, 2000; Warrell et al., 1988). In some cases, this leads to a serious complication, known as cerebral malaria, which is associated with coma and neurological sequalae (Renia et al., 2012). It remains unclear to what extent the decreased deformability of infected RBCs contributes directly to trapping of infected RBCs.

*P. knowlesi* is a parasite of long-tailed macaques (*Macaca fascicularis*) that causes zoonotic infections in humans and is the most common cause of human malaria in Malaysia (Singh & Daneshvar, 2013). It is associated with high parasitemia infections and causes severe malaria in adult humans at a rate similar to *P. falciparum* (Barber et al., 2013; Cox-Singh & Singh, 2008). *P. knowlesi* expresses the antigenic variant, SICAvar (Howard, Barnwell, & Kao, 1983), but its role in pathogenesis remain uncertain. *P. knowlesi*-infected RBCs also exhibit decreased host cell deformability (Barber, Russell et al., 2018) and splenic rupture has been observed, suggesting blockage of sinusoidal vessels (Chang, Pui, Kadir, & Singh, 2018), while an autopsy of a fatal human knowlesi malaria case revealed brain capillaries congested with infected RBCs (Menezes et al., 2012). Acute kidney injury, potentially caused by chronic haemolysis, also contributes to severe pathology (Barber, Grigg, et al., 2018). The molecular basis for the different pathologies remains poorly understood (Renia et al., 2012).

Altered cellular properties are also observed in immature RBCs, known as reticulocytes. The earliest enucleated reticulocyte forms are released from the bone marrow with extra surface area and an elevated membrane shear modulus (Liu, Guo, Mohandas, Chasis, & An, 2010; Malleret et al., 2013). The transition of reticulocytes to mature RBCs is accompanied by the loss of surface area, acquisition of a biconcave shape and increased deformability (Li et al., 2018). The consequences of the lower deformability of early stage reticulocytes on passage through small capillaries is not well studied.

Over the past few decades, many studies have examined the biomechanical properties of healthy and diseased RBCs using a variety of tools. Techniques such as micropipette aspiration, atomic force microscopy, optical tweezers, quantitative phase imaging, dynamic light scattering, ektacytometry, filtration and microfluidic devices have been used to study the behaviour of individual RBCs and populations of RBCs (Kim, Kim, & Park, 2012). These different techniques show different sensitivities to contributions from RBC geometry, cytoplasmic viscosity and plasma membrane viscoelasticity, making it difficult to correlate in vitro measures of biomechanical properties with clinical pathologies (Ataga et al., 2011; Huisjes et al., 2018; Nader et al., 2019; Renoux et al., 2019).

In this work, we have re-examined the usefulness of ektacytometry as a measure of deformability. Ektacytometry measures the ability of RBCs to elongate upon application of shear stress in fluid flow. Membrane viscoelasticity and cytoplasmic viscosity are known to be important determinants of the ability of RBCs to elongate (Diez-Silva et al., 2010; Mohandas & Gallagher, 2008; Pivkin et al., 2016), but the individual contributions from these parameters often cannot be discriminated. Here, we use the term 'cellular viscoelasticity' to refer to the physicochemical properties that determine the ability of RBCs to elongate under flow. While the contribution of SA:V ratio to the rheological behaviour of RBCs is generally well established, its particular effect on the ability of RBCs to elongate in flow is less well studied.

Another physiologically relevant parameter is the ability of RBCs to passage into small constrictions, which is expected to have consequences for transfer through very narrow capillaries and splenic fenestrations (Kim et al., 2012; Safeukui et al., 2018). However, the individual effects of cell geometry and cellular viscoelasticity on capillary traversal are not well understood.

In this study, we monitored RBC traversal into an array of microchannels, with diameters commensurate with the smallest vessels in the circulation and examined the effects of independently manipulating cellular viscoelasticity and SA:V ratio. As examples of physiological and pathological changes to RBC membrane properties, we examined the traversal of reticulocytes and *P. falciparum*- and *P. knowlesi*-infected RBCs. We developed a computational model and used it to help understand the contributions from different parameters and to estimate the minimum pressure required to force RBCs with different SA:V ratios and viscoelasticity properties through small capillaries, mimicking the dimension of those in the cerebral cortex.

## 2 | RESULTS

### 2.1 | Calibrating measurements of RBC geometry

We employed a modified version of the microfluidic device called a Human Erythrocyte Microchannel Analyser (HEMA; Gifford

et al., 2003) to assess the ability of RBCs to traverse into wedge-shaped microchannels. Scanning electron microscopy (SEM) images of a chip are presented in Figure S1. RBCs enter the ~5 μm diameter opening and become trapped before reaching the 1.4 μm exit (Figure 1a). The position where the RBC becomes lodged represents the smallest diameter of an equivalent cylindrical tube through which the RBC can pass. We use a previously coined term, minimum cylindrical diameter (MCD; Canham & Burton, 1968; Herricks, Antia, & Rathod, 2009) to describe this parameter. Subtle differences in the way MCD is calculated in our study are detailed in section 3.3.1. Conforming the RBCs into the microchannels allows estimation of the cell surface area and volume (Gifford et al., 2003; Herricks et al., 2009; Lelliott et al., 2017; see section 3.3 for details).

It was important to determine the variability in the measurements, which could be affected by batch-to-batch differences in microchannel dimensions. We analysed the same batch of RBCs in five independently fabricated chips, revealing small variations in estimates of MCD (Figure 1b). In an effort to obtain a reliable estimate of the different geometrical parameters, we averaged data from eight different experiments (2,562 RBCs). This analysis reveals an average volume of 99 ± 12 fL and an average surface area of 149 ± 14 $\mu m^2$, giving a SA:V ratio of 1.50 ± 0.12. The average MCD is 3.03 ± 0.21 μm (Figure 1b). The data are in good agreement with previous reports (Gifford et al., 2003; Hanssen et al., 2012; Herricks et al., 2009; Park et al., 2008). Nonetheless, given the degree of variation, where possible we examined different samples in the same chip by differentially labelling one population or washing and reusing the chip for different samples on the same day. In some experiments, the values were normalised to untreated RBCs.

## 2.2 | Decreased cellular viscoelasticity limits RBC elongation but not traversal into microchannels

We first examined the behaviour of RBCs under conditions in which the cellular viscoelasticity was modified by chemical treatment, but the SA:V ratio was held as constant as possible. Glutaraldehyde is a non-specific cross-linking agent that stiffens the cell membrane by cross-linking membrane proteins, and increases cellular viscosity by cross-linking haemoglobin (Forsyth, Wan, Ristenpart, & Stone, 2010). RBCs were treated for 1 hr with different glutaraldehyde concentrations. We consider this composite change in properties as a decrease in cellular viscoelasticity.

We used a RheoScan Ektacytometer (Shin, Ku, Park, & Suh, 2005) to measure the elongation index (EI) of RBCs at shear stresses ranging from 0 to 20 Pa. RBCs were mixed with 6% polyvinylpyrrolidone (PVP) in buffer prior to analysis. Ektacytometry revealed a marked decrease in EI as the glutaraldehyde concentration increased from 0.001 to 0.005% (Figure 1c). The mean shear stress has been estimated to be 2–4 Pa in small venules and 6–8 Pa in arterioles (Ballermann, Dardik, Eng, & Liu, 1998). Thus, our data indicate that at physiologically relevant shear stresses, the ability of the RBCs treated with 0.004% glutaraldehyde to elongate is largely abrogated (Figure 1c).

For HEMA analysis, glutaraldehyde-treated RBCs and control (unfixed) RBCs were mixed in phosphate-buffered saline (PBS) at a ratio of 1:1 and introduced into the microfluidic chip. Fixed RBCs were identified by an increased autofluorescence signal (Figure 1a). Different chips were used for the three glutaraldehyde concentrations examined and the data were normalised to the untreated RBCs in the same chip.

No significant changes in volume or surface area, and thus SA:V ratio, were observed between fixed and unfixed RBCs at glutaraldehyde concentrations of 0.001 and 0.004% (Figure 1d). (The actual values for the SA:V ratio are provided in Figure S2a.) These data show that markedly stiffened RBCs (0.004% glutaraldehyde) retain the ability to conform to the shape of the narrowing microchannel, reaching an MCD of 3.00 ± 0.23 μm, similar to unfixed RBCs (3.02 ± 0.21 μm; $p = .54$; 95% confidence interval: −0.075 to 0.039; $n = 279$ unfixed RBCs, 76 fixed RBCs). These data show that cellular viscoelasticity has little impact on RBC traversal into small microchannels.

Treatment with 0.005% glutaraldehyde increases the MCD to 3.19 ± 0.31 μm, which is significantly larger than for unfixed RBCs measured in the same chip (3.02 ± 0.22 μm; $p < .00001$; 95% confidence interval: 0.11–0.24; $n = 257$ unfixed RBCs, 104 fixed RBCs; Figure 1d). In this case, however, the surface area, and thus SA:V ratio, appears to be decreased compared with unfixed RBCs (Figure 1e; Figure S2). This difference emanates from the formation of creases in the membrane (see Figure 1a), causing an underestimation of the surface area. No creases were observed in the membranes of RBCs fixed with lower glutaraldehyde concentrations or in unfixed RBCs (seeFigure S3).

## 2.3 | SA:V ratio limits traversal of RBCs into microchannels but has less effect on elongation

We next examined the impact of altered cell volume on microchannel traversal and RBC elongation, by varying the osmolarity of the buffering solution from 139 to 484 mOsm/L. At higher or lower osmolarities, the ability of RBCs to elongate in flow decreased substantially (Figure 2a), in agreement with previous data (Clark, Mohandas, & Shohet, 1983; Renoux et al., 2019). However, at osmolarities relatively close to the physiological range (Gennari, 1984), 239–350 mOsm/L, the EI showed relatively little dependence on osmolarity (Figure 2a, red box). We examined RBC behaviour over the same range, using a single HEMA device, with flushing of the device between experiments. We observed a gradual decrease in cell volume and a slight apparent increase in cell surface area as the cells dehydrate and shrink in the increasing buffer osmolarity (Figure 2b,c; Figure S4). The resultant increase in SA:V ratio (from 1.38 ± 0.11 to 1.58 ± 0.10; Figure 2d) is associated with a decrease in the MCD value from 3.29 ± 0.24 μm (239 mOsm/L; $n = 411$ RBCs) to 2.89 ± 0.15 μm (350 mOsm/L; $n = 423$ RBCs; $p < .00001$; 95% confidence interval: 0.37–0.43; Welch two samples $t$ test; Figure 2e).

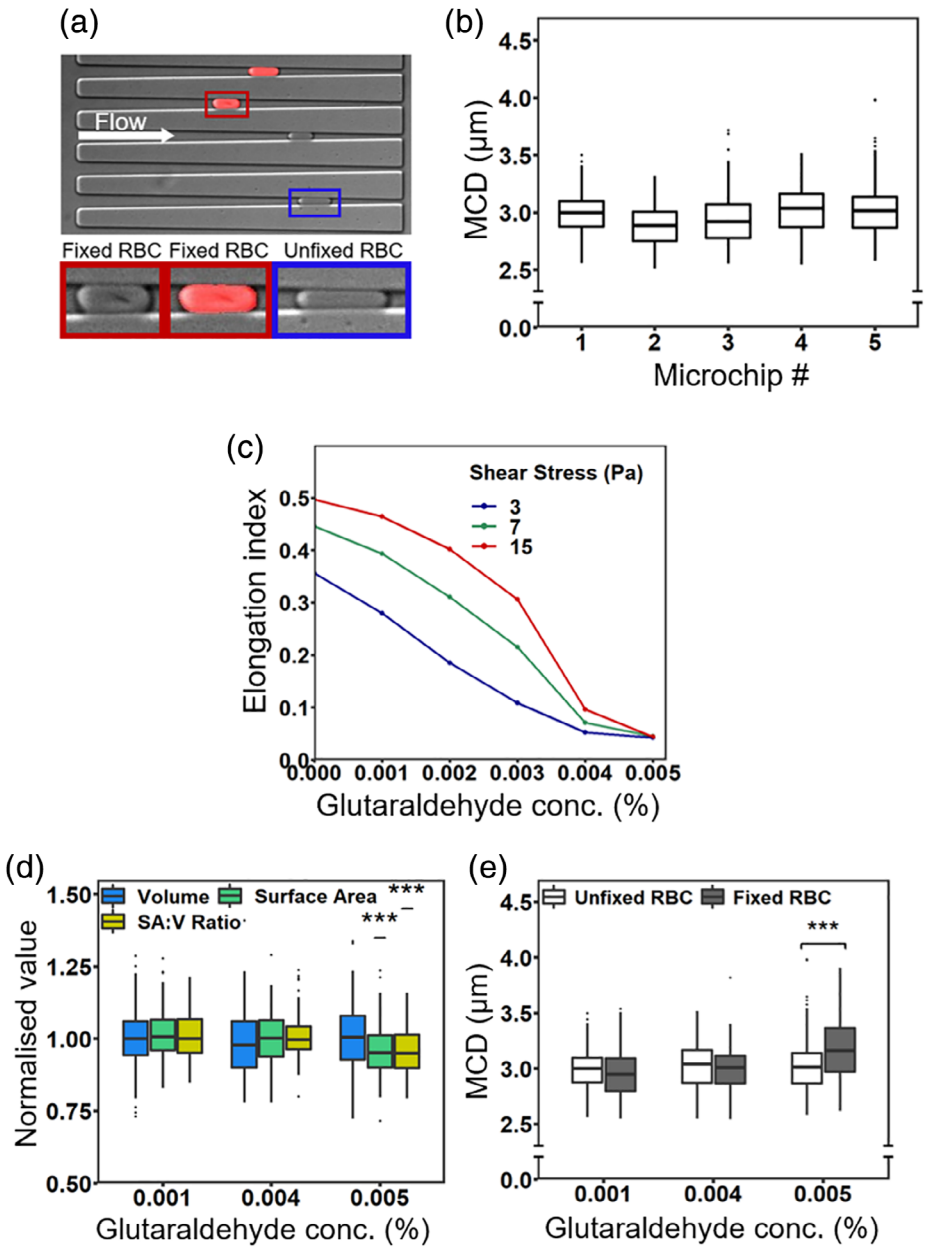



**FIGURE 1** Ektacytometry and Human Erythrocyte Microchannel Analyser (HEMA) analyses of unfixed and fixed red blood cells (RBCs). (a) A mixed population of untreated RBCs and RBCs treated with 0.005% glutaraldehyde were driven into the wedge-shaped microchannels in the HEMA chip. The image shows fixed RBCs (red autofluorescence) in the top two channels, with one cell (red box) showing a crease (see higher magnification inset with and without fluorescence overlay). Unfixed RBCs (Channels 3 and 5) are arrested further along the channels. One cell (blue box) is shown at higher magnification in the inset. (b) Comparison of the minimum cylindrical diameter (MCD) for healthy RBCs examined in five different HEMA chips. (c) Comparison of the elongation index (EI) for RBCs treated with glutaraldehyde, at shear stresses of 3, 7 and 15 Pa. (d) Normalised values of SA:V ratio for fixed and unfixed RBCs. Individual data points indicate the full range of values. Data represent a single experiment. An additional experiment using blood from a different donor is presented in Figure S2b,c. (e) Mean MCD values ± *SD* for unfixed RBCs (white) and fixed RBCs (grey). ***$p < .001$; compared with unfixed RBCs; Welch two samples *t* test

Indeed, a roughly inverse linear relationship was observed between MCD and SA:V ratio (Figure S4).

## 2.4 | SA:V ratio is the main determinant of microchannel traversal for malaria parasite-infected RBCs

We next examined the importance of SA:V ratio and cellular visco-elasticity in determining microchannel traversal of parasitised RBCs. RBCs infected with *P. falciparum* (3D7) trophozoites (32–36 hr) were magnet-purified and washed in complete (serum-containing) culture medium and analysed by ektacytometry at a parasitemia level of 98%. The infected RBCs exhibit a markedly decreased ability to undergo elongation compared with uninfected RBCs (Figure 3a). Indeed, *P. falciparum*-infected RBCs exhibited an elongation index profile similar to that for RBCs treated with 0.005% glutaraldehyde.

For the HEMA experiments, we directly compared uninfected and infected RBCs in the same chip. We used the highly absorbing hemozoin crystals to identify infected RBCs (Figure 3b). It should be noted that the MCD for uninfected RBCs in complete culture medium (MCD = 2.81 ± 0.15; $n$ = 1,528 RBCs) was moderately lower than for RBCs suspended in PBS (MCD = 3.03 ± 0.21; $n$ = 2,562 RBCs; $p < .00001$; 95% confidence interval: −0.23 to −0.21), potentially due to nutrient or serum albumin effects.

We observed no significant difference in the mean SA:V ratio of *P. falciparum* trophozoites compared to uninfected RBCs, measured in

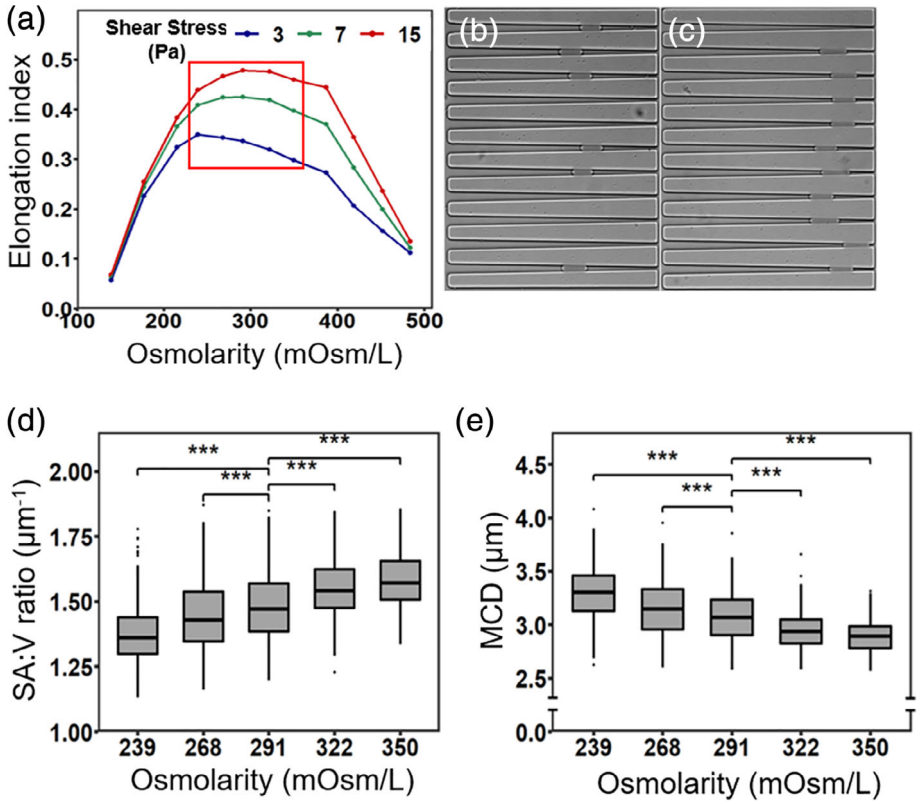



**FIGURE 2** Ektacytometry and HEMA analyses of RBCs subjected to different osmolarities. (a) Elongation index as a function of the medium osmolarity at shear stresses of 3, 7 and 15 Pa. The red box indicates osmolarities, 239–350 mOsm/L, relatively close to the physiological range. (b, c) Images of the wedge-shaped microchannels with arrested RBCs in media with osmolarities of 239 mOsm/L (b) and 350 mOsm/L (c). (d,e) Mean values SA:V ratio and MCD for RBCs subjected to different osmolarities. ***$p$ < .001; compared with the RBCs subjected to the buffer osmolarity of 291 mOsm/L; Welch two samples $t$ test. All five conditions were examined in a single HEMA chip, starting from 239 mOsm/L. After each experiment, the chip was flushed with the next buffer for 30 min before re-introducing the RBCs. The data are from a single experiment and are typical of two experiments performed using blood from different donors. HEMA, Human Erythrocyte Microchannel Analyser; MCD, minimum cylindrical diameter; RBCs, red blood cells

the same chip (Figure 3c–f), in agreement with some previous reports (Hanssen et al., 2012; Liu et al., 2019; Waldecker et al., 2017). Despite the very limited ability of *P. falciparum* trophozoite-infected RBCs to elongate in fluid flow and the presence of a parasite inside the host cell, infected RBCs were able to traverse to the same MCD value (2.78 ± 0.18; $n$ = 529) as uninfected RBCs (2.79 ± 0.15; $n$ = 1,038; $p$ = .18; 95% confidence interval: −0.029 to 0.0056; five experiments; Figure 3f). The same behaviour was observed for RBCs infected with trophozoites of another strain of *P. falciparum* (CS2; Figure S5).

We also examined RBCs infected with *P. knowlesi* trophozoites (22–26 hr). Magnet-purified infected RBCs (in serum-containing culture medium) were analysed by ektacytometry at a parasitemia level of 97%. *P. knowlesi*-infected RBCs show reduced ability to elongate in flow (Figure 3g), but appeared less rigid than *P. falciparum*-infected RBCs. *P. knowlesi* trophozoite-infected RBCs exhibit an increased volume (∼23%) and surface area (∼12%) compared to uninfected RBCs, leading to a ∼9% decrease in the SA:V ratio (Figure 3i–k). Accordingly, the *P. knowlesi*-infected RBCs (MCD 3.08 ± 0.23; $n$ = 406 RBCs) were less able to traverse microchannels than uninfected RBCs (MCD 2.84 ± 0.13; $n$ = 490 RBCs; $p$ < .00001; 95% confidence interval: 0.21–0.26; three experiments; Figure 3h,l). These data are consistent with a previous study that used broader stage windows (Liu et al., 2019) and confirm that SA:V ratio is a more important determinant than cellular viscoelasticity of the ability of RBCs to traverse small microchannels, with implications for the pathology of *P. knowlesi* infections.

## 2.5 | Reticulocytes have an equivalent SA:V ratio to mature RBCs and traverse microchannels with similar efficiency despite lower cellular viscoelasticity

Immature RBCs, known as reticulocytes, have a higher surface area and a higher shear modulus than mature RBCs (Malleret et al., 2013). Here, we purified reticulocytes by centrifugation on a Percoll cushion. Block-face SEM revealed the larger size and lobed nature of the reticulocytes (Figure S6; see Video S1 for rotations of the models). The reticulocyte fraction contains a variable population of more mature RBCs [negative for the Thiazole Orange RNA stain and/or CD71 (i.e., transferrin receptor)]. The EI at 3 Pa of reticulocyte-enriched samples (80% RNA positive, 59% CD71+) was approximately 13% lower than for mature RBCs ($n$ = 3, representative plot in Figure 4a), consistent with previous reports of a twofold higher shear modulus, as measured by micropipette aspiration (Malleret et al., 2013).

For the HEMA analysis, the reticulocyte fraction (66% RNA positive, 33% CD71+) was labelled with an antibody recognising CD71, which is lost during maturation (Kono, Kondo, Takagi, Wada, & Fujimoto, 2009). Mature RBCs retrieved from the Percoll pellet fraction were counter-labelled with an antiserum recognising complement receptor-1 (CR1), which is present on all maturation stages. The reticulocyte fraction (CD71+ and CD71−) and mature RBCs were mixed and introduced into the HEMA device in PBS (Figure 4b). (It should be noted that the CD71- population may include a percentage of contaminating mature RBCs.) The volume and surface area of CD71+ reticulocytes were each found to be ∼30% higher than for mature

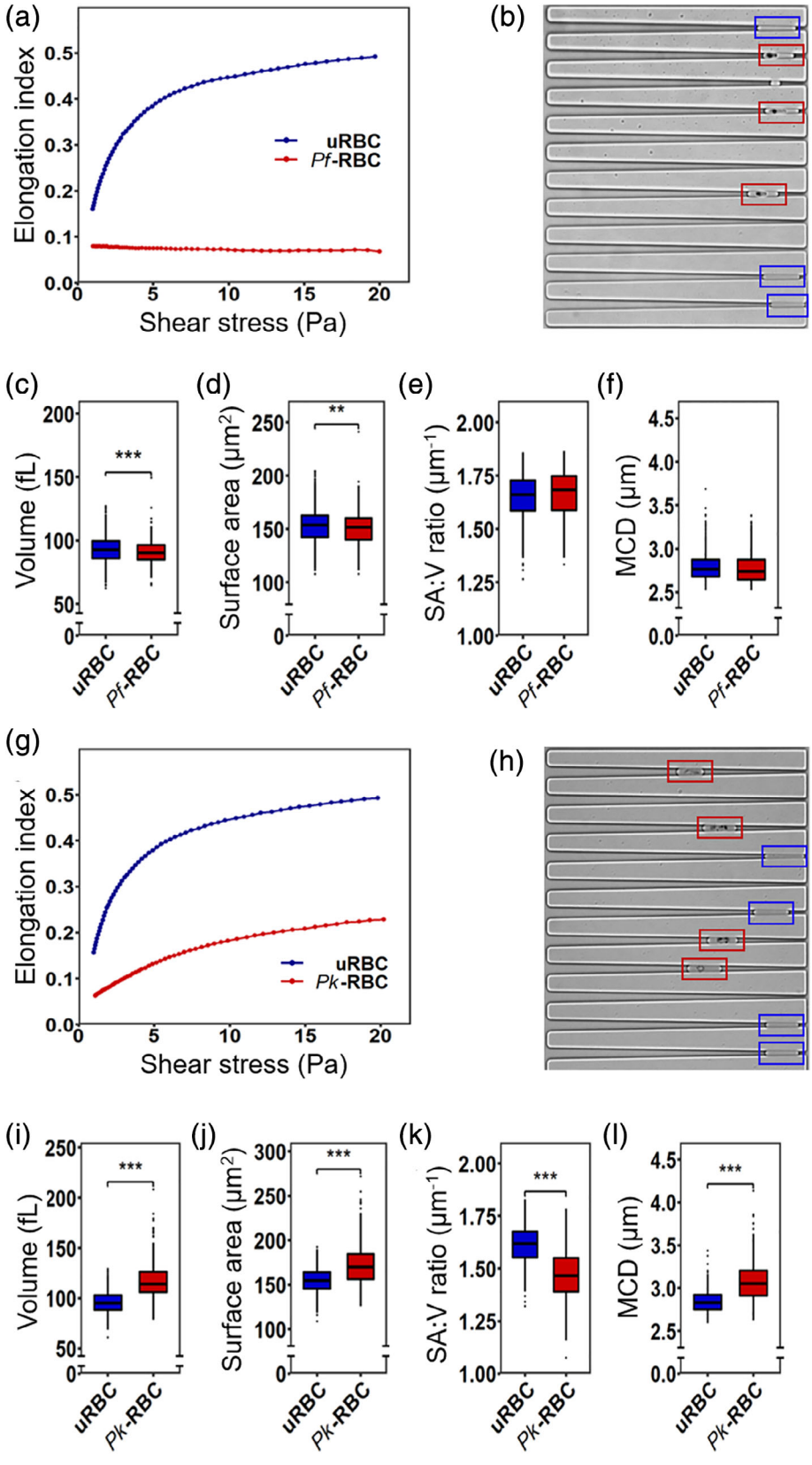



**FIGURE 3** Ektacytometry and HEMA analyses of parasitised RBCs. (a,g) Ektacytometry (0–20 Pa shear stress) of uninfected RBCs (blue lines) and RBCs infected with *P. falciparum* (a; 32–36 hr) or *P. knowlesi* (g; 22–26 hr, red lines). (b,h) RBCs infected with *P. falciparum* (b) or *P. knowlesi* (h) (red boxes) and uninfected RBCs (blue boxes) were trapped in wedge-shaped microchannels. Mean values of volume, surface area, SA:V ratio and MCD for RBCs infected with *P. falciparum* (c–f, red) or *P. knowlesi* (i–l, red) and uninfected RBCs (blue). ***$p < .001$; compared with uninfected RBCs; Welch two samples *t* test. The data represent combined results from five independent experiments for *P. falciparum* and three independent experiments for *P. knowlesi* using blood from different donors. HEMA, Human Erythrocyte Microchannel Analyser; MCD, minimum cylindrical diameter; RBCs, red blood cells

RBCs (Figure 4c,d), while CD71− reticulocytes exhibited intermediate sizes. Despite the difference in size, both CD71+ and CD71− reticulocytes exhibit the same SA:V ratio as mature RBCs (Figure 4e) and were found to reach the same MCD (Figure 4f; CD71+ reticulocyte MCD = 3.09 ± 0.18, $n = 168$; mature RBC MCD = 3.10 ± 0.15, $n = 69$; $p$ value = .79; 95% confidence interval: −0.052 to 0.039).

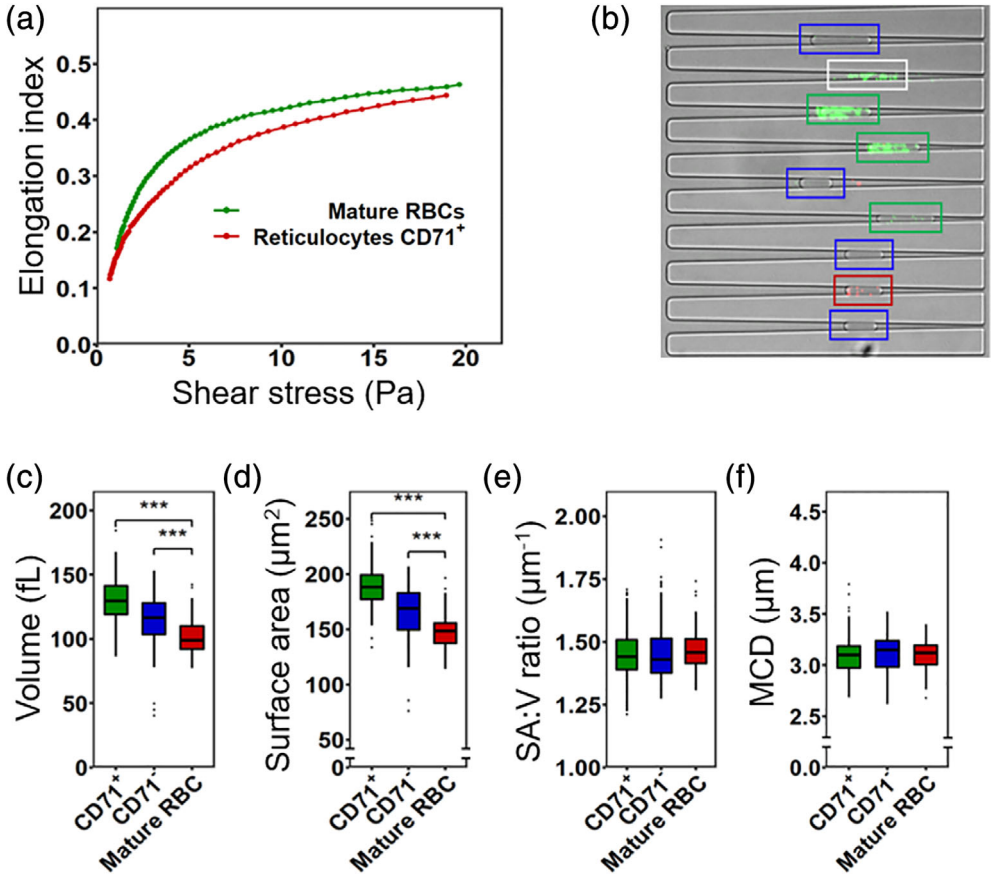



**FIGURE 4** Ektacytometry and HEMA analyses of reticulocytes. (a) Ektacytometry (0–20 Pa shear stress) of uninfected RBCs (red line) and purified cord blood reticulocytes (80% RNA+, of which 59% are RNA+/CD71+; green line). (b) Mature RBCs were labelled for CR1 (647, red boxes) and reticulocytes (purified from whole blood; 66% total RNA+, of which 33% are RNA+/CD71+) for CD71 (488, green boxes). Unlabelled cells are assumed to be CD71− cells from the reticulocyte fraction (blue boxes) but may include some mature RBCs. Some lysed cell membranes, as evident by loss of refraction in the bright field images, are visible in the channels (white box). (e, f) Comparison of mean values of volume (c), surface area (d), SA:V ratio (e) and MCD (f) for mature RBCs (red), intermediate stages (CD71−, blue) and reticulocytes (CD71+, green). ***$p < .001$; compared with mature RBCs; Welch two samples $t$ test. The data are from a single experiment and are typical of experiments performed three times using blood from different donors. HEMA, Human Erythrocyte Microchannel Analyser; MCD, minimum cylindrical diameter; RBCs, red blood cells

## 2.6 | A 3D computational model of RBCs traversing the HEMA microchannels

We developed a biomechanical simulation model of RBC traversal into the HEMA chip to estimate the forces that RBCs would experience, and to probe the physical basis for the importance of SA:V ratio on RBC traversal through narrow microchannels. We deployed the commercial Abaqus software (SIMULIA, Providence, RI) to generate a nonlinear 3D Finite Element (FE) model (Figure 5a), building on previous studies (Aingaran et al., 2012; Mills, Qie, Dao, Lim, & Suresh, 2004). The membrane was modelled using the third-order Yeoh hyper-elastic model (Yeoh, 1990) with an initial in-plane shear modulus of $\mu_0$ = 7.3 μN/m for healthy RBCs, based on reported values (Mills et al., 2004; Yoon & You, 2016). We employed an initial SA:V ratio value of 1.54, based on our own initial estimate of SA:V ratio. For consistency with previously generated models (Evans & Fung, 1972), we also examined a SA:V ratio of 1.42 (Figures S7 and S9). Further details of the model can be found in the section 3.3.2.

At any given point in the HEMA device, an RBC undergoes a complex distribution of stresses that cannot be measured experimentally. Thus, we resorted to estimating the pressure that an RBC would experience using our FE model and HEMA measurements of deformed length and diameter of healthy RBCs. An RBC is subjected to a net force along the flow direction when it is introduced to the microchip due to the pressure difference (drop) across the cell surface. The pressure drop per cell increases as the RBC squeezes into the narrowing microchannel, and the pressure drop reaches its maximum once the cell is trapped. To estimate the pressure drop per RBC in the wedge-shaped channels, we applied a range of pressures to the HEMA simulation and found that a pressure drop of 2.20 Pa per cell best fits our experimental measurements on the untreated RBCs (Figure S7). The estimated pressure drop value is similar to that

reported in previous studies (Aingaran et al., 2012; Pivkin et al., 2016). All subsequent simulations of the HEMA experiments on chemically treated RBCs were conducted with the estimated pressure drop of 2.20 Pa.

## 2.7 | Simulation of the effect of membrane viscoelasticity on RBC traversal into a microchannel

We carried out two numerical analyses of RBCs within the HEMA device, considering (a) only membrane viscoelasticity variation, and (b) only SA:V ratio variation. We have employed the constraint of a constant surface area and cell volume. The in-plane membrane shear modulus is reported to be in the range of 5–10 μN/m for normal RBCs (Evans, Mohandas, & Leung, 1984; Hochmuth & Waugh, 1987), increasing to ~40 μN/m for trophozoite stage *P. falciparum*-infected RBCs, and to as high as 90 μN/m at the schizont stage (Park et al., 2008; Suresh et al., 2005). RBCs infected with mature stage *P. knowlesi* exhibit a membrane shear modulus of 45 μN/m (Barber, Russell, et al., 2018).

We simulated variation of in-plane membrane shear modulus with values from 7.3 to 109.5 μN/m and examined the MCD reached for RBCs with a constant SA:V ratio of 1.54 (Figure 5c). RBCs exhibiting a shear modulus up to 50 μN/m were trapped in the microchannels at an MCD of 3.1 μm (Figure 5c), which is similar to the experimentally determined value for RBCs with the equivalent SA:V ratio (Figure 2e). RBCs exhibiting a shear modulus greater than 50 μN/m exhibit a moderate decrease in traversal into the microchannels. For instance, an RBC exhibiting a shear modulus of 109.5 μN/m exhibited a ~6% larger MCD than a healthy cell. Creases formed in the cell membrane in the simulations when the membrane shear modulus was higher than 73 μN/m (Figure 5b), similar to those observed experimentally in RBCs treated with 0.005% glutaraldehyde. The simulation is consistent with our experimental observation that a dramatic increase in the

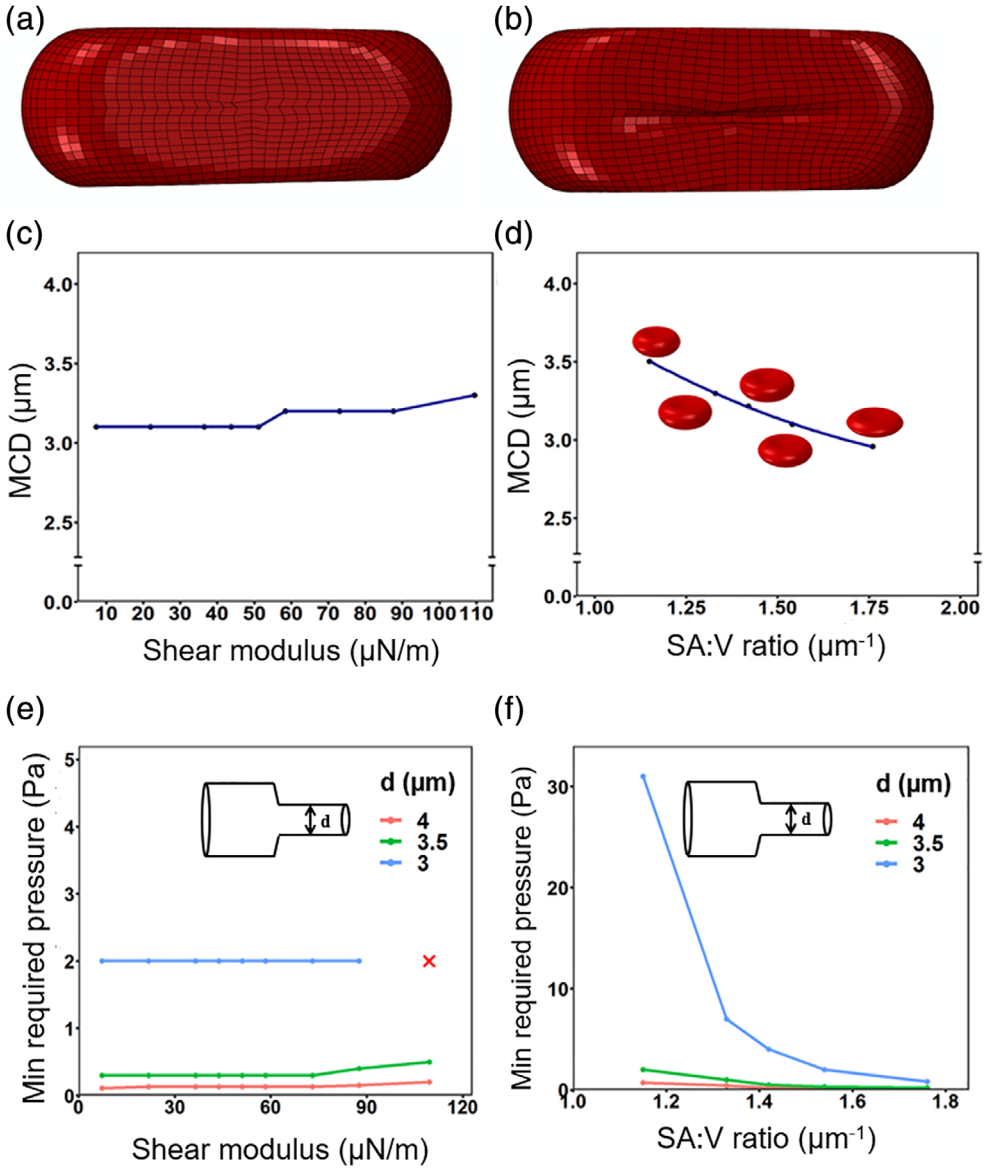



**FIGURE 5** Numerical simulations of RBC passage through microchannels and capillaries. (a,b) Deformed shapes of red blood cells (RBCs) subjected to $\mu$ = 7.3 μN/m (a) and $\mu$ = 73 μN/m (b), showing strain around creases in the membrane. (c) Minimum cylindrical diameter (MCD) reached by RBCs in the microchannels as a function of increasing membrane shear modulus. (d) MCD reached by RBCs at SA:V ratios of 1.15–1.76. (e,f) Simulations of RBC traversal in small capillaries (3–4 μm). The minimum required pressure is predicted for RBCs with different membrane shear moduli (e) and SA:V ratios (f)

membrane shear modulus has only a moderate effect on RBC traversal into the microchannels. The range of stresses and strains in the membrane at the various shear moduli is presented in Figure S8. We also examined the effect of membrane viscoelasticity on the passage of RBCs with a SA:V ratio of 1.42 (Figure S9).

## 2.8 | Simulation of the effect of SA:V ratio on RBC traversal into a microchannel

Simulations were performed on RBCs with different SA:V ratios, ranging from 1.15 to 1.76. These RBC models were generated by altering the geometrical parameters in the standard geometry formula (Evans & Fung, 1972). The volumes of the generated cells were varied from 117 to 78 fL, while keeping the surface area constant (134 $\mu m^2$) and the membrane shear modulus constant ($\mu_0$ = 7.3 μN/m). The MCD decreased as the SA:V ratio increased (Figure 5d), consistent with the observation that the passage of RBCs into the microchannels is highly dependent on the SA:V ratio. The range of stresses and strains in the membrane at the different SA:V ratios is detailed in Figure S8. The stresses experienced are low at physiologically relevant SA:V ratio but increase rapidly as the SA:V ratio decreases. For instance, the maximum von Mises stress in the membrane is quadrupled to 950 Pa when the SA:V ratio of the RBC is decreased from 1.54 to 1.15. Our simulations suggest that the MCD for an RBC with a surface area of 134 $\mu m^2$, and known SA:V ratio, can be estimated using the formula:

$$\mathrm{MCD} = 0.56(\mathrm{SA:V\,ratio})^2 - 2.54\,(\mathrm{SA:V\,ratio}) + 5.68 \qquad (1)$$

## 2.9 | Prediction of RBC passage in channels with the dimension of cerebral capillaries

We used our whole cell FE model to predict whether high membrane viscoelasticity or low SA:V ratio would restrict the passage of a population of RBCs through the smallest capillaries encountered under patho/physiological conditions, which may have diameters as low as 3 μm (Canham & Burton, 1968; Lauwers et al., 2008; Linninger et al., 2013). In this work, we found that the average MCD for healthy RBCs suspended in PBS is 3.03 ± 0.21 μm (average of ~2,562 RBCs from different experiments). It should be noted, however, that the 90 percentile values for MCD are 2.73 and 3.29 μm. We performed simulations to evaluate the minimum required pressure for RBCs with a SA:V ratio of 1.54 to squeeze into small capillaries with diameters of 3, 3.5 and 4 μm (Figure 5e,f). RBCs pass through the 3.5 and 4 μm capillaries, even under very low pressures; however, a higher pressure (~2 Pa) was required to drive RBCs through the 3 μm channel. Decreased membrane viscoelasticity did not affect the minimum required pressure for RBCs to pass through these small capillaries (Figure 5e). All stiffened cells except the one with the highest shear modulus (109.5 μN/m) can pass the minimum diameter capillary (3 μm) by applying a pressure drop of 2 Pa. We also examined the minimum required pressure for RBCs with a SA:V ratio of 1.42 and different levels of membrane viscoelasticity (Figure S9). Again, shear modulus is not an important determinant.

In contrast, the minimum required pressure steeply increases as the SA:V ratio decreases, most strikingly for the 3 μm channel. For RBCs with a SA:V ratio less than 1.4, a marked increase in the pressure is required to drive traversal through the 3 μm capillary (Figure 5f). Our simulations show that RBCs with a low SA:V ratio are more prone to trapping in small capillaries than cells with low viscoelasticity.

# 3 | DISCUSSION

RBCs need to undergo severe deformation to pass through narrow capillaries and fenestrations; and their ability to do so can be compromised in different physiological and pathological conditions (Safeukui et al., 2018; Suzuki, Tateishi, Soutani, & Maeda, 1996; Tomaiuolo, 2014). In this work, we examined the individual contributions of cellular viscoelasticity and geometry on the ability of RBCs to conform into microchannels. We made use of a modified version of the HEMA microfluidic device (Gifford et al., 2003) in which RBCs are flowed into wedge-shaped microchannels. Conforming RBCs into the microchannels allows estimation of the surface area, the volume and the MCD, that is, the diameter of the smallest equivalent cylindrical tube through which an RBC could pass. Small variations in channel geometry were observed between different HEMA chips and, where possible, we examined different samples in the same chip by differentially labelling one population or washing and reusing the chip for different samples on the same day.

We altered the SA:V ratio of RBCs by modifying the buffer osmolarity. In agreement with previous reports (Gifford et al., 2003; Reinhart & Chien, 1985; Safeukui et al., 2012), we found that the ability of RBCs to travel into microchannels is highly sensitive to the SA:V ratio. Our experiments revealed a roughly inverse relationship between MCD and SA:V ratio. Importantly, in the SA:V range close to physiological levels, that is, 1.38–1.58, the 15% increase in MCD was readily detected by HEMA. By contrast, we found that ektacytometry, a method that is often used to measure RBC defects, was quite insensitive to changes in the SA:V ratio over this range.

Somewhat surprisingly, substantial decreases in cellular viscoelasticity did not affect the ability of RBCs to progress into the channels. For this work, we used glutaraldehyde, a bifunctional linker that cross-links membrane proteins, thereby decreasing the shear modulus, as well as polymerising haemoglobin, thus increasing cytoplasmic viscosity. Treatment with 0.004% glutaraldehyde largely abrogated the ability of RBCs to elongate in fluid flow. Such changes in the rheological properties of the RBCs would be expected to markedly increase blood viscosity at high shear stress, which would adversely affect the rheology of bulk flow (Mohandas & Gallagher, 2008; Pivkin et al., 2016). By contrast, these highly rigidified cells migrated to a similar position in the microchannels as untreated RBCs. These data suggest that cellular

viscoelasticity plays a less important role in passage through very narrow channels than generally appreciated.

To examine the consequences of our findings for different pathological conditions, we examined the biomechanical properties of RBCs infected with two different species of malaria parasite that are expected to induce a complex combination of changes to cellular viscoelasticity. We found that RBCs infected with *P. falciparum* in the trophozoite stage of infection are highly rigidified, exhibiting no elongation in fluid flow, even at the highest applied shear stress, similar to the behaviour of RBCs treated with the highest glutaraldehyde concentration. This is likely due to the greatly increased shear modulus of the host RBC membrane (Park et al., 2008; Suresh et al., 2005), as well as the presence of an intracellular trophozoite, which occupies about 50% of the host cell cytoplasm (Hanssen et al., 2012). In our work, we found that *P. falciparum* trophozoite-infected RBCs maintained the same SA:V ratio as uninfected RBCs. Some other studies have reported that *P. falciparum*-infected RBCs exhibit a decreased SA:V ratio (Herricks et al., 2009; Safeukui et al., 2012). This discrepancy may arise from differences in the methods used to assess SA:V ratio, or from the fact that previous studies examined RBCs infected with more mature schizont stage parasites, which undergo permeability changes leading up to parasite egress (Hale et al., 2017). Further work is needed to determine what factors influence the MCD of *P. falciparum*-infected RBCs and whether there are systematic differences between parasite strains and/or culture conditions that underpin the differences between different laboratories.

Our work suggests that the rigidification of trophozoite-stage infected RBCs is not, in and of itself, sufficient to hinder passage through microcapillaries. Similarly, the presence of the intracellular parasite, with a volume of up to ~50 fL, does not increase the MCD. This suggests that the intracellular trophozoite must exhibit sufficient deformability to be able to conform to the shape of the channel. Nonetheless, rigidification of the RBC membrane will enhance adhesion to microvessel walls by distributing the tensional forces imposed on individual adhesin molecules through to the membrane skeletal network (Zhang et al., 2015). Adherent *P. falciparum*-infected RBCs may narrow the blood vessels, leading to increased microvascular obstruction and downstream clinical complications (Hanson et al., 2015).

Our results have important implications for *P. knowlesi* infections. In Malaysia, *P. knowlesi* now accounts for >90% of all malaria cases (Cooper et al., 2020). Severe *P. knowlesi* malaria is associated with haemolysis-induced endothelial activation leading to acute kidney injury (Barber, Grigg, et al., 2018; Grigg et al., 2018). We found that *P. knowlesi*-infected RBCs exhibit a large increase in volume and a more moderate increase in surface area, resulting in an overall decrease in SA:V ratio and a consequent increase in MCD. We anticipate that the increased MCD of *P. knowlesi*-infected cells will contribute to sequestration within the vasculature (Knisely, Stratman-Thomas, Eliot, & Bloch, 1964; Menezes et al., 2012). We also note that *P. knowlesi*-infected RBCs exhibit surface expression of the variant antigen, SICAvar (Lapp, Korir, & Galinski, 2009) and some strains are reported to bind in vitro to the endothelial ligand, ICAM-1 (Fatih et al., 2012). Thus, host cell swelling and adhesion may both contribute to sequestration. The consequent evasion of the splenic clearance mechanisms may enable increased parasite density. The increased volume may also underpin the finding that *P. knowlesi*-infected RBCs are hyper-sensitive to hypotonic lysis (Liu et al., 2019). Chronic intravascular rupture of swollen *P. knowlesi*-infected RBCs may lead to chronic release of haem and iron (Van Avondt, Nur, & Zeerleder, 2019), which may in turn lead to the acute kidney injury that characterises severe knowlesi malaria.

We also examined the geometry and biomechanical properties of early stage reticulocytes. When first released from the bone marrow, reticulocytes contain RNA and have remnant surface receptors, particularly the transferrin receptor, CD71, which can be labelled with antibodies. As the reticulocyte matures, CD71 is lost via a process of shedding and endocytosis. In the final stages of maturation the RNA is degraded (Malleret et al., 2013; Mankelow et al., 2015). We used CD71 labelling of density gradient-purified reticulocytes to identify early stage reticulocytes and found that they have 30% more surface area than mature RBCs. This difference is larger than reported in previous studies that detected reticulocytes based on RNA staining (Gifford, Derganc, Shevkoplyas, Yoshida, & Bitensky, 2006; Waugh et al., 1997). Our data confirm that a loss of surface area accompanies the loss of surface markers. In agreement with previous studies, we found that reticulocytes exhibit a decreased ability to elongate in fluid flow. Nonetheless, even the early stage (CD71+) reticulocytes exhibit a very similar SA:V ratio to mature RBCs, which likely underpins their ability to passage through the microcirculation without disturbing blood flow.

We generated a nonlinear 3D FE model to further interrogate the biomechanical basis for our surprising finding that cellular viscoelasticity makes very little contribution to the ability of RBCs to traverse small channels. These simulations are consistent with our experimental observations. The RBC membrane skeleton imparts extremely nonlinear mechanical behaviour (Mills et al., 2004), which means that the RBC can still conform to the microchannel even when the viscoelasticity decreases. At very high shear modulus values, we observed the formation of creases in the membrane that prevent the RBC from travelling into smaller equivalent diameters, as strain and stress in the membrane are significantly increased in the vicinity of the creases. Importantly, our simulations are consistent with the experimental finding that a moderate decrease in the SA:V ratio, that is, moderately increased RBC sphericity, markedly affects its ability to traverse small channels. We note, as a limitation of our study, that we did not consider time-dependent parameters, such as the rate of progress of RBCs in the microchannels, prior to being trapped. Further work is needed to understand the effects of changes to RBC physical properties on the blood flow rate and viscosity.

We were able to use our FE model to predict cut-off values for shear modulus and SA:V ratio that would prevent RBCs passing through small channels with diameters comparable to cerebral cortex capillaries. These values are difficult to obtain experimentally. Our analysis reveals that stiffening the RBCs has relatively little effect on the minimum applied pressure needed to force RBCs to passage

through capillaries, even of 3 μm diameter. Thus, even highly rigidified RBCs would be expected to passage through the microcirculation, so long as the SA:V ratio is kept constant. By contrast, reducing the SA:V ratio to 1.2 increases the minimum applied pressure by ∼15-fold.

We note that while our work provides insights into the determinants of passage of modified RBCs through small capillaries, they do not address the biomechanical parameters that permit passage through splenic endothelial slits, which can be as narrow as 1–2 μm. Further work is needed to measure and model the individual effects of cellular viscoelasticity and SA:V ratio on this important biomechanical surveillance mechanism.

In summary, we have employed a modified HEMA microfluidic device that enables accurate determination of volume, surface area and the capillary diameter through which an RBC can passage. We found that RBC cellular viscoelasticity makes very little contribution to RBC behaviour during passage through small channels due to the nonlinear mechanical behaviour of the RBC membrane skeleton (Mills et al., 2004). Our work has particular implications for diseases such as hereditary spherocytosis and hereditary elliptocytosis (Da Costa et al., 2016; Warkentin, Barr, Ali, & Mohandas, 1990) that exhibit a decreased SA:V ratio. Following splenectomy – a treatment that is commonly used to reduce anaemia – circulation of RBCs with decreased SA:V ratio may impair blood flow through small capillaries, contributing to an enhanced risk of thrombosis (Byrnes & Wolberg, 2017; Cappellini et al., 2000; Iolascon et al., 2017; Schilling, Gangnon, & Traver, 2008). Application of techniques that are highly sensitive to changes in SA:V ratio may provide an important indicator of the pathological consequences of changes in RBC geometry.

## 4 | EXPERIMENTAL PROCEDURES

### 4.1 | Glutaraldehyde treatment

Glutaraldehyde (Sigma, EM grade) solutions in PBS were prepared at the required concentration. O+ human RBCs (Red Cross Blood Band, Australia) were gently dispersed at 2% haematocrit and incubated at room temperature (RT) for 1 hr. The RBCs were pelleted at 300*g* for 2 min, resuspended in PBS and washed three times. The treated cells were mixed at a 1:1 ratio with untreated cells from the same RBC aliquot before introduction to the microfluidic device. Treated cells were identified by their autofluorescence in long-exposure images collected with 632 nm excitation/676 (34) nm emission filter sets.

### 4.2 | Altering buffer osmolarity

The buffer osmolarity was tuned over the range 150–520 mOsm/kg by adjusting the NaCl content while keeping the $Na_2HPO_4$, $KH_2PO_4$ and KCl concentrations constant at 10, 1.8 and 2.7 mM respectively. The pH was adjusted to 7.35 before measurement of osmolarity using an Advanced Instruments 3320 freezing-point osmometer. RBCs were washed once in PBS before being dispersed in osmolarity-modified PBS at 2% haematocrit. RBC suspensions were further diluted with modified PBS before introduction to the microfluidic device.

### 4.3 | Culture of *P. falciparum* and *P. knowlesi*

*P. falciparum* (3D7 strain; intra-erythrocytic cycle of ∼43 hr duration) and *P. knowlesi* (A1 strain; intra-erythrocytic cycle of ∼32 hr duration; Moon et al., 2013) were cultured as described previously (Liu et al., 2019). Briefly, parasites were maintained in O+ human RBCs (5% haematocrit) in RPMI-based complete medium containing pooled human serum (5%), AlbuMAX II (5%), 200 μM hypoxanthine, 10 mM D-glucose (Sigma) and 20 μg/ml gentamicin (Sigma). Parasitemia was routinely maintained below 5%. Synchronised trophozoite-stage infected RBCs (32–36 hr post-invasion *P. falciparum*; 22–26 hr post-invasion *P. knowlesi*) were enriched from culture by magnetic separation (Liu et al., 2019) and assessed for stage in Giemsa-stained smears.

### 4.4 | Reticulocyte purification

Five hundred millilitre of whole blood (Australian Red Cross) or 80 ml cord blood (BMDI Cord Blood Bank) was passed through an RC High Efficiency leucocyte removal filter (Haemonetics Australia) and washed three times with PBS to remove serum components. Donated blood was approved for use by the Walter and Eliza Hall Institute Human Research Ethics Committee (HREC 14/09). RBCs at approximately 50% haematocrit were layered onto a 70% (vol/vol) isotonic Percoll cushion (GE Healthcare) and centrifuged for 25 min at 2000*g*. The thin band formed at the Percoll interface was collected as the reticulocyte fraction, while the pellet was collected as the mature cell fraction. The percentage of reticulocytes in the reticulocyte fraction was measured by flow cytometry. Reticulocyte preparations (∼$10^7$ cells/ml) were incubated for half an hour with 100 μl thiazole orange (TO; Retic-Count Reagent; BD Biosciences) and Alexa-647 conjugated mouse mAb against transferrin receptor (CD71, mouse mAb MEM75, Abcam ab187777). The RBCs were washed with PBS then resuspended in 200 μl PBS and analysed on the FACSCalibur flow cytometer (BD Biosciences). A total of 50,000 events were recorded and analysed using FlowJo software (Three Star). Cells were stored in RPMI wash buffer (Gibco) at 4°C until needed. Reticulocytes were identified in HEMA experiments by labelling with antisera for CD71 (mouse mAb 13E4, Abcam ab38171) and anti-mouse Alexa-488 secondary. Pelleted (mature) RBCs were tagged by labelling with antisera against complement receptor-1 (CD35, mouse mAb543), and anti-mouse Alexa 647 secondary. Labelling was performed at 1:500 in PBS solution with 3% bovine serum albumin for 1 hr at RT followed by at least three washing steps in PBS. Mature and immature cell types were mixed at a ratio of 1:3 following labelling before introduction to the HEMA device. Unlabelled cells were considered to be CD71-reticulocytes, however this fraction may also include unlabelled (CD35–) mature

cells. For all experiments, the mature RBC fraction analysed refers to mature RBCs collected from the same preparation.

## 4.5 | Ektacytometry

An aliquot of packed RBCs (10 μl) was dispersed into 500 μl of 6% 360 kDa PVP in PBS. The EI was measured using a RheoScan Ektacytometer (Dearnley et al., 2016; Shin et al., 2005), at stress stresses of 0–20 Pa, covering low and high stress conditions (Dobbe, Streekstra, Hardeman, Ince, & Grimbergen, 2002; Sosa, Nielsen, Vignes, Chen, & Shevkoplyas, 2014). Each measurement was performed in triplicate and the averaged data are presented. Infected RBCs were magnet-purified (parasitemia >97%) before analysis.

## 4.6 | Fabrication of HEMA microfluidic chips

Our microchannel arrays are based on a modified original design (Gifford et al., 2003) and are fabricated using standard soft lithography (Lake et al., 2015; Madou, 2002). Briefly, polydimethyl-siloxane (PDMS) elastomer is applied to a pre-fabricated master mould (Melbourne Centre for Nanofabrication) and cured in an oven. Holes punched into the PDMS before glass coverslip attachment allow for connection of tubing to a fluid reservoir and pressure pump. The microchannels were 125.2±0.06 μm long and 3.23±0.05 μm deep as measured via SEM. The width of wedge-shaped microchannels was 4.98 ±0.07 μm at the entrance and 1.44±0.04 μm at the exit. Small variations in geometry were observed between different HEMA chips.

## 4.7 | SEM imaging

PDMS containing the HEMA pattern was cut to size and into cross-sections with a razor blade before mounting on conducting carbon tape. PDMS sections were sputter coated from a gold target to a thickness of ~0.5 nm before measurement. Reticulocytes and mature RBCs were pre-fixed in 0.005% glutaraldehyde in PBS for 20 min at RT before full fixation in 2.5% glutaraldehyde in PBS for 1.5 hr at RT. Agarose-embedded cells were stained in ferrocyanide-reduced osmium tetroxide in 0.15M cacodylate buffer for 1 hr on ice. After washing, the preparation was incubated with freshly prepared 1% thiocarbonhydrazide solution in $H_2O$ for 20 min at RT, stained with 2% osmium tetroxide in $H_2O$ for 30 min at RT, stained with 1% aqueous uranyl acetate overnight followed by Walton's lead aspartate for 30 min at 60°C. The preparation was dehydrated in a graded series of ethanol-$H_2O$, followed by progressive infiltration with EPON resin. After polymerisation, the resin block was trimmed, mounted on a microtome stub using silver glue on an ultramicrotome (UC7, Leica). The resin block face was polished again with a diamond knife on the ultramicrotome after 10 nm gold coating. Serial images were collected using a serial block face-scanning electron microscope (SBF-SEM), equipped with an in-chamber diamond knife (Teneo VolumeScope, FEI Company), using the back-scattered electron signal at 3 kV, under low vacuum conditions. The section thickness was set to 50 nm and the pixel size of each image in the stack was 5 nm. Serial sections were contrasted and aligned using IMOD software (Boulder Laboratory for 3D Electron Microscopy of Cells). Raw images were binned to 20 nm and smoothed with a Gaussian function before segmentation using contours and thresholding.

## 4.8 | HEMA experimental setup

The HEMA chip was purged (using a syringe pump) with 80% ethanol at a flow rate of 2 μl/min for 30 min, then flushed with PBS or complete culture media for 45 min. Diluted washed blood (at 0.2–0.5% haematocrit) was driven into the microchannels at a flow pressure of 180–250 mbar using an Elveflow AF1 pressure pump. Experiments were completed within 1 hr, as infected cells trapped in the device were prone to lysis. Due to a slight variability in dimensions from device to device, for all experiments except the glutaraldehyde study, the same microchip was used for several samples. The microfluidic channels were backflushed with PBS for 20 min at a flow rate of 3 μl/min before flushing with the new buffer for 30 min between each sample. Microfluidic chips were mounted in a Deltavision Elite (GE Healthcare) inverted microscope and imaged using a ×40 air objective at 37°C for malaria parasite-infected cells and at RT for other experiments. Images were collected in brightfield along with the blue fluorescence channel (390/18 nm excitation and 435/48 nm collection filter sets) to facilitate automated analysis using the shadow of RBC haemoglobin in the fluorescence images.

## 4.9 | Determination of surface area and volume

To calculate the volume and surface area of each arrested RBC, four points were accurately delineated on each cell: (a) the left-most point of each cell, (b) the point where the cell touches the wall, (c) the point where the cell is detached from the wall and (d) the right-most point of the cell. These points were automatically located in acquired images using a macro plugin developed in ImageJ. By measuring the distances of each of these four points from the narrow end of microchannels, the mid-point position ($d_{mid}$), the height of the end caps ($h_{lc}$ and $h_{rc}$) and the length of the main body ($L_b$) of each arrested cell can be calculated as follows:

$$d_{mid} = \frac{d_A + d_D}{2} \quad (2)$$

$$L_b = d_B - d_C \quad (3)$$

$$h_{lc} = (d_A - d_B), h_{rc} = (d_C - d_D) \quad (4)$$

It was previously reported (Gifford et al., 2003) that arrested cells do not fully fill the rectangular cross-section of the wedge-shaped

channels, and some space between the arrested cells and the corners of the microchannels are left unfilled. $R_C$ represents an effective radius of the cell cross-section, simplifying the two caps of the arrested RBC as spherical caps smoothly fitted to main body of the cell, and $R_E$ is the radius of rounded corners of the cell cross-section.

An empirical relationship between $R_E$ and the cell position in the wedge-shaped channels was previously established (Gifford et al., 2003):

$$R_E = 0.385\,\mu m + 0.008 \times d_{mid} \quad (5)$$

By calculating $R_E$ and the geometry of wedge-shaped microchannels ($\alpha$ = .82°), $R_C$ can also be calculated using Equation (6)

$$R_C = \sqrt{\left(\frac{Depth}{2} - R_E\right)^2 + \left(\frac{Width}{2} - R_E\right)^2} + R_E \quad (6)$$

For simplicity, $R_C$ is assumed constant all along the arrested RBC. Then, the area ($Area_s$) and circumference ($Circ_s$) of the cell cross-section can be calculated as follows:

$$Area_s = Width \times Depth - 4 \times \left(1 - \frac{\pi}{4}\right) R_E^2 \quad (7)$$

$$Circ_s = 4 \times \left(\frac{2\pi R_E}{4}\right) + 2 \times (Width - 2R_E) + 2 \times (Depth - 2R_E) \quad (8)$$

Finally, we calculated the volume and surface area of each arrested RBC using Equations (9) and (10).

$$Volume = (L_b \times Area_s) + \frac{\pi}{6}\left(3R_C^2 + h_{lc}^2\right) L_{lc} + \frac{\pi}{6}\left(3R_C^2 + h_{rc}^2\right) L_{rc} \quad (9)$$

$$Surface\ Area = (L_b \times Circ_s) + \pi\left(R_C^2 + h_{lc}^2\right) + \pi\left(R_C^2 + h_{rc}^2\right) \quad (10)$$

## 4.10 | MCD calculation

MCD is calculated as the cross-sectional area ($Area_m$) of an arrested RBC at its midpoint (Equation 11).

$$MCD = 2 \times \sqrt{\frac{Area_m}{\pi}} \quad (11)$$

## 4.11 | 3D FE model

The RBC membrane was discretised using four-node linear shell elements, and the third-order Yeoh hyper-elastic model was used to represent the stress–strain relationships in the membrane. For all computations, a typical bending modulus of $2 \times 10^{-19}$ Nm was assumed (Mills et al., 2004; Yoon & You, 2016). Cytosol, an incompressible fluid inside the membrane, keeps the cell volume constant under the deformation. Thus, we regarded the cytosol as a volume constant constraint inside the cell membrane and ran all the simulations using the quasi-static analysis. Blood vessel walls are reported to be two to three orders of magnitude stiffer than RBCs (Lu, Yang, Zhao, Gregersen, & Kassab, 2003; Xie, Zhou, & Fung, 1995). Therefore, we ignored deformation of the capillary wall and regarded the capillaries as rigid parts in the FE model. The modelled wedge-shaped microchannel has a length of 125 μm, with a width of 4.9 μm at the opening and 1.1 μm at the exit.

## 4.12 | Statistics and reproducibility

Statistical analysis employed the Welch two samples *t* test (R software). Each of the presented dataset are representative of or averages of data obtained during at least two different experimental sessions, using different batches of blood, as detailed in the text.

### ACKNOWLEDGEMENTS

The authors thank the Australian Red Cross Blood Service for whole blood. Cord blood units were supplied by the BMDI Cord Blood Bank at the Murdoch Childrens Research Institute and The Royal Children's Hospital. Establishment and running of the BMDI Cord Blood Bank is made possible through generous support by Federal and state governments, the Murdoch Childrens Research Institute, The Royal Children's Hospital Foundation and the Fight Cancer Foundation. The authors also thank Sebastien Menant, the Walter and Eliza Hall Institute for help with preparation of reticulocytes. Light microscopy was performed at the Biological Optical Microscopy Platform and electron microscopy at the Bio21 Institute Advanced Microscopy Facility, The University of Melbourne (www.microscopy.unimelb.edu.au). This work was performed in part at the Melbourne Centre for Nanofabrication (MCN) in the Victorian Node of the Australian National Fabrication Facility (ANFF). This work was supported by the National Health & Medical Research Council of Australia and the Australia Research Council.

### CONFLICT OF INTEREST

The authors declare no conflict of interest.

### AUTHOR CONTRIBUTIONS

**Leann Tilley**, **Vijay Rajagopal**, **Arman Namvar**, **Adam J. Blanch**, **Peter V. S. Lee**, **Matthew W. Dixon:** Designed the study. **Arman Namvar**, **Adam J. Blanch**, **Boyin Liu:** Performed the experiments. **Arman Namvar**, **Adam J. Blanch**, **Vijay Rajagopal**, **Matthew W. Dixon:** Analysed the data. **Olivia M. S. Carmo**, **Snigdha Tiash**, **Oliver Looker**, **Dean Andrew**, **Li-Jin Chan**, **Wai-Hong Tham:** Characterised and provided the samples. **Leann Tilley**, **Vijay Rajagopal**, **Arman Namvar**, **Adam J. Blanch**, **Peter V. S. Lee**, **Matthew W. Dixon:** Wrote the article. All authors participated in discussion and paper editing.

## DATA AVAILABILITY STATEMENT

The data that support the findings of this study are available from the corresponding author upon reasonable request.

## ORCID

*Wai-Hong Tham* https://orcid.org/0000-0001-7950-8699
*Vijay Rajagopal* https://orcid.org/0000-0002-5509-402X
*Leann Tilley* https://orcid.org/0000-0001-9910-0199

## REFERENCES

Aingaran, M., Zhang, R., Law, S. K., Peng, Z., Undisz, A., Meyer, E., … Marti, M. (2012). Host cell deformability is linked to transmission in the human malaria parasite *Plasmodium falciparum*. *Cellular Microbiology*, *14*, 983–993.

Allison, A. C. (1960). Turnovers of erythrocytes and plasma proteins in mammals. *Nature*, *188*, 37–40.

An, X., & Mohandas, N. (2008). Disorders of red cell membrane. *British Journal of Haematology*, *141*, 367–375.

Ataga, K. I., Reid, M., Ballas, S. K., Yasin, Z., Bigelow, C., James, L. S., … *ICA-17043-10 Study Investigators*. (2011). Improvements in haemolysis and indicators of erythrocyte survival do not correlate with acute vaso-occlusive crises in patients with sickle cell disease: A phase III randomized, placebo-controlled, double-blind study of the Gardos channel blocker senicapoc (ICA-17043). *British Journal of Haematology*, *153*, 92–104.

Ballermann, B. J., Dardik, A., Eng, E., & Liu, A. (1998). Shear stress and the endothelium. *Kidney International*, *67*, S100–S108.

Barber, B. E., Grigg, M. J., Piera, K. A., William, T., Cooper, D. J., Plewes, K., … Anstey, N. M. (2018). Intravascular haemolysis in severe *Plasmodium knowlesi* malaria: Association with endothelial activation, microvascular dysfunction, and acute kidney injury. *Emerging Microbes & Infections*, *7*, 106.

Barber, B. E., Russell, B., Grigg, M. J., Zhang, R., William, T., Amir, A., … Yeo, T. W. (2018). Reduced red blood cell deformability in *Plasmodium knowlesi* malaria. *Blood Advances*, *2*, 433–443.

Barber, B. E., William, T., Grigg, M. J., Menon, J., Auburn, S., Marfurt, J., … Yeo, T. W. (2013). A prospective comparative study of *knowlesi*, *falciparum*, and *vivax* malaria in Sabah, Malaysia: High proportion with severe disease from Plasmodium *knowlesi* and *Plasmodium vivax* but no mortality with early referral and artesunate therapy. *Clinical Infectious Diseases*, *56*, 383–397.

Beare, N. A., Harding, S. P., Taylor, T. E., Lewallen, S., & Molyneux, M. E. (2009). Perfusion abnormalities in children with cerebral malaria and malarial retinopathy. *The Journal of Infectious Diseases*, *199*, 263–271.

Byrnes, J. R., & Wolberg, A. S. (2017). Red blood cells in thrombosis. *Blood*, *130*, 1795–1799.

Canham, P. B., & Burton, A. C. (1968). Distribution of size and shape in populations of normal human red cells. *Circulation Research*, *22*, 405–422.

Cappellini, M. D., Robbiolo, L., Bottasso, B. M., Coppola, R., Fiorelli, G., & Mannucci, A. P. (2000). Venous thromboembolism and hypercoagulability in splenectomized patients with thalassaemia intermedia. *British Journal of Haematology*, *111*, 467–473.

Chang, C. Y., Pui, W. C., Kadir, K. A., & Singh, B. (2018). Spontaneous splenic rupture in *Plasmodium knowlesi* malaria. *Malaria Journal*, *17*, 448.

Clark, M., Mohandas, N., & Shohet, S. (1983). Osmotic gradient ektacytometry: Comprehensive characterization of red cell volume and surface maintenance. *Blood*, *61*, 899–910.

Cooper, D. J., Rajahram, G. S., William, T., Jelip, J., Mohammad, R., Benedict, J., … Barber, B. E. (2020). *Plasmodium knowlesi* malaria in Sabah, Malaysia, 2015-2017: Ongoing increase in incidence despite near-elimination of the human-only *Plasmodium* species. *Clinical Infectious Diseases*, *70*, 361–367.

Cox-Singh, J., & Singh, B. (2008). Knowlesi malaria: Newly emergent and of public health importance? *Trends in Parasitology*, *24*, 406–410.

Da Costa, L., Suner, L., Galimand, J., Bonnel, A., Pascreau, T., Couque, N., … Mohandas, N. (2016). Diagnostic tool for red blood cell membrane disorders: Assessment of a new generation ektacytometer. *Blood Cells, Molecules & Diseases*, *56*, 9–22.

de Koning-Ward, T. F., Dixon, M. W., Tilley, L., & Gilson, P. R. (2016). Plasmodium species: Master renovators of their host cells. *Nature Reviews. Microbiology*, *14*, 494–507.

Dearnley, M., Chu, T., Zhang, Y., Looker, O., Huang, C., Klonis, N., … Tilley, L. (2016). Reversible host cell remodeling underpins deformability changes in malaria parasite sexual blood stages. *Proceedings of the National Academy of Sciences of the United States of America*, *113*, 4800–4805.

Diez-Silva, M., Dao, M., Han, J., Lim, C. T., & Suresh, S. (2010). Shape and biomechanical characteristics of human red blood cells in health and disease. *MRS Bulletin*, *35*, 382–388.

Dobbe, J. G., Streekstra, G. J., Hardeman, M. R., Ince, C., & Grimbergen, C. A. (2002). Measurement of the distribution of red blood cell deformability using an automated rheoscope. *Cytometry*, *50*, 313–325.

Dondorp, A. M., Kager, P. A., Vreeken, J., & White, N. J. (2000). Abnormal blood flow and red blood cell deformability in severe malaria. *Parasitology Today*, *16*, 228–232.

Evans, E., & Fung, Y.-C. (1972). Improved measurements of the erythrocyte geometry. *Microvascular Research*, *4*, 335–347.

Evans, E., Mohandas, N., & Leung, A. (1984). Static and dynamic rigidities of normal and sickle erythrocytes. Major influence of cell hemoglobin concentration. *The Journal of Clinical Investigation*, *73*, 477–488.

Fatih, F. A., Siner, A., Ahmed, A., Woon, L. C., Craig, A. G., Singh, B., … Cox-Singh, J. (2012). Cytoadherence and virulence – The case of *Plasmodium knowlesi* malaria. *Malaria Journal*, *11*, 33.

Forsyth, A. M., Wan, J., Ristenpart, W. D., & Stone, H. A. (2010). The dynamic behavior of chemically "stiffened" red blood cells in microchannel flows. *Microvascular Research*, *80*, 37–43.

Gennari, F. J. (1984). Current concepts. Serum osmolality. Uses and limitations. *The New England Journal of Medicine*, *310*, 102–105.

Gifford, S. C., Derganc, J., Shevkoplyas, S. S., Yoshida, T., & Bitensky, M. W. (2006). A detailed study of time-dependent changes in human red blood cells: From reticulocyte maturation to erythrocyte senescence. *British Journal of Haematology*, *135*, 395–404.

Gifford, S. C., Frank, M. G., Derganc, J., Gabel, C., Austin, R. H., Yoshida, T., & Bitensky, M. W. (2003). Parallel microchannel-based measurements of individual erythrocyte areas and volumes. *Biophysical Journal*, *84*, 623–633.

Glenister, F. K., Coppel, R. L., Cowman, A. F., Mohandas, N., & Cooke, B. M. (2002). Contribution of parasite proteins to altered mechanical properties of malaria-infected red blood cells. *Blood*, *99*, 1060–1063.

Grigg, M. J., William, T., Barber, B. E., Rajahram, G. S., Menon, J., Schimann, E., … Anstey, N. M. (2018). Age-related clinical spectrum of *Plasmodium knowlesi* malaria and predictors of severity. *Clinical Infectious Diseases*, *67*, 350–359.

Hale, V. L., Watermeyer, J. M., Hackett, F., Vizcay-Barrena, G., van Ooij, C., Thomas, J. A., … Saibil, H. R. (2017). Parasitophorous vacuole poration precedes its rupture and rapid host erythrocyte cytoskeleton collapse in *Plasmodium falciparum* egress. *Proceedings of the National Academy of Sciences of the United States of America*, *114*, 3439–3444.

Hanson, J., Lee, S. J., Hossain, M. A., Anstey, N. M., Charunwatthana, P., Maude, R. J., … Dondorp, A. M. (2015). Microvascular obstruction and endothelial activation are independently associated with the clinical manifestations of severe falciparum malaria in adults: An observational study. *BMC Medicine*, *13*, 122.

Hanssen, E., Knoechel, C., Dearnley, M., Dixon, M. W., Le Gros, M., Larabell, C., & Tilley, L. (2012). Soft X-ray microscopy analysis of cell volume and hemoglobin content in erythrocytes infected with asexual and sexual stages of *Plasmodium falciparum*. *Journal of Structural Biology*, *177*, 224–232.

Herricks, T., Antia, M., & Rathod, P. K. (2009). Deformability limits of *Plasmodium falciparum*-infected red blood cells. *Cellular Microbiology*, *11*, 1340–1353.

Hochmuth, R. M., & Waugh, R. E. (1987). Erythrocyte membrane elasticity and viscosity. *Annual Review of Physiology*, *49*, 209–219.

Howard, R. J., Barnwell, J. W., & Kao, V. (1983). Antigenic variation of *Plasmodium knowlesi* malaria: Identification of the variant antigen on infected erythrocytes. *Proceedings of the National Academy of Sciences of the United States of America*, *80*, 4129–4133.

Huisjes, R., Bogdanova, A., van Solinge, W. W., Schiffelers, R. M., Kaestner, L., & van Wijk, R. (2018). Squeezing for life – Properties of red blood cell deformability. *Frontiers in Physiology*, *9*, 656.

Iolascon, A., Andolfo, I., Barcellini, W., Corcione, F., Garçon, L., De Franceschi, L., … Working Study Group on Red Cells Iron of the E. H. A. (2017). Recommendations regarding splenectomy in hereditary hemolytic anemias. *Haematologica*, *102*, 1304–1313.

Kim, Y., Kim, K., & Park, Y. (2012). Measurement techniques for red blood cell deformability: Recent advances. In T. E. Moschandreou (Ed.), *Blood cell – An overview of studies in hematology*. Rijeka, Croatia: IntechOpen.

Knisely, M. H., Stratman-Thomas, W. K., Eliot, T. S., & Bloch, E. H. (1964). Knowlesi malaria in monkeys II: A first step in the separation of the mechanical pathologic circulatory factors of one sludge disease from possible specific toxic factors of that disease. *Angiology*, *15*, 411–416.

Kono, M., Kondo, T., Takagi, Y., Wada, A., & Fujimoto, K. (2009). Morphological definition of CD71 positive reticulocytes by various staining techniques and electron microscopy compared to reticulocytes detected by an automated hematology analyzer. *Clinica Chimica Acta*, *404*, 105–110.

Kuhn, V., Diederich, L., Keller, T. C. S. T., Kramer, C. M., Luckstadt, W., Panknin, C., … Cortese-Krott, M. M. (2017). Red blood cell function and dysfunction: Redox regulation, nitric oxide metabolism, anemia. *Antioxidants & Redox Signaling*, *26*, 718–742.

Lake, M., Narciso, C., Cowdrick, K., Storey, T., Zhang, S., Zartman, J. and Hoelzle, D.J.P.E. (2015). Microfluidic device design, fabrication, and testing protocols 10.

Lapp, S. A., Korir, C. C., & Galinski, M. R. (2009). Redefining the expressed prototype SICAvar gene involved in *Plasmodium knowlesi* antigenic variation. *Malaria Journal*, *8*, 181.

Lauwers, F., Cassot, F., Lauwers-Cances, V., Puwanarajah, P., & Duvernoy, H. (2008). Morphometry of the human cerebral cortex microcirculation: General characteristics and space-related profiles. *NeuroImage*, *39*, 936–948.

Lelliott, P. M., Huang, H. M., Dixon, M. W., Namvar, A., Blanch, A. J., Rajagopal, V., … Burgio, G. (2017). Erythrocyte beta spectrin can be genetically targeted to protect mice from malaria. *Blood Advances*, *1*, 2624–2636.

Li, H., Yang, J., Chu, T. T., Naidu, R., Lu, L., Chandramohanadas, R., … Karniadakis, G. E. (2018). Cytoskeleton remodeling induces membrane stiffness and stability changes of maturing reticulocytes. *Biophysical Journal*, *114*, 2014–2023.

Linninger, A. A., Gould, I. G., Marrinan, T., Hsu, C. Y., Chojecki, M., & Alaraj, A. (2013). Cerebral microcirculation and oxygen tension in the human secondary cortex. *Annals of Biomedical Engineering*, *41*, 2264–2284.

Liu, B., Blanch, A. J., Namvar, A., Carmo, O., Tiash, S., Andrew, D., … Tilley, L. (2019). Multimodal analysis of *Plasmodium knowlesi*-infected erythrocytes reveals large invaginations, swelling of the host cell, and rheological defects. *Cell Microbiology*, *21*(5), e13005.

Liu, J., Guo, X., Mohandas, N., Chasis, J. A., & An, X. (2010). Membrane remodeling during reticulocyte maturation. *Blood*, *115*, 2021–2027.

Lu, X., Yang, J., Zhao, J. B., Gregersen, H., & Kassab, G. S. (2003). Shear modulus of porcine coronary artery: Contributions of media and adventitia. *American Journal of Physiology-Heart and Circulatory Physiology*, *285*, H1966–H1975.

Madou, M. J. (2002). *Fundamentals of microfabrication: The science of miniaturization*. Boca Raton: CRC Press.

Malleret, B., Xu, F., Mohandas, N., Suwanarusk, R., Chu, C., Leite, J. A., … Russell, B. (2013). Significant biochemical, biophysical and metabolic diversity in circulating human cord blood reticulocytes. *PLoS One*, *8*, e76062.

Mankelow, T. J., Griffiths, R. E., Trompeter, S., Flatt, J. F., Cogan, N. M., Massey, E. J., & Anstee, D. J. (2015). Autophagic vesicles on mature human reticulocytes explain phosphatidylserine-positive red cells in sickle cell disease. *Blood*, *126*, 1831–1834.

Mankelow, T. J., Satchwell, T. J., & Burton, N. M. (2012). Refined views of multi-protein complexes in the erythrocyte membrane. *Blood Cells, Molecules & Diseases*, *49*, 1–10.

Marin-Padilla, M. (2012). The human brain intracerebral microvascular system: Development and structure. *Frontiers in Neuroanatomy*, *6*, 38.

Menezes, R. G., Pant, S., Kharoshah, M. A., Senthilkumaran, S., Arun, M., Nagesh, K. R., … Fazil, A. (2012). Autopsy discoveries of death from malaria. *Legal Medicine (Tokyo, Japan)*, *14*, 111–115.

Mills, J. P., Qie, L., Dao, M., Lim, C. T., & Suresh, S. (2004). Nonlinear elastic and viscoelastic deformation of the human red blood cell with optical tweezers. *Mechanics & Chemistry of Biosystems*, *1*, 169–180.

Mohandas, N., & Gallagher, P. G. (2008). Red cell membrane: Past, present, and future. *Blood*, *112*, 3939–3948.

Moon, R. W., Hall, J., Rangkuti, F., Ho, Y. S., Almond, N., Mitchell, G. H., … Blackman, M. J. (2013). Adaptation of the genetically tractable malaria pathogen *Plasmodium knowlesi* to continuous culture in human erythrocytes. *Proceedings of the National Academy of Sciences of the United States of America*, *110*, 531–536.

Nader, E., Skinner, S., Romana, M., Fort, R., Lemonne, N., Guillot, N., … Connes, P. (2019). Blood rheology: Key parameters, impact on blood flow, role in sickle cell disease and effects of exercise. *Frontiers in Physiology*, *10*, 1329.

Park, Y., Diez-Silva, M., Popescu, G., Lykotrafitis, G., Choi, W., Feld, M. S., & Suresh, S. (2008). Refractive index maps and membrane dynamics of human red blood cells parasitized by *Plasmodium falciparum*. *Proceedings of the National Academy of Sciences of the United States of America*, *105*, 13730–13735.

Pivkin, I. V., Peng, Z., Karniadakis, G. E., Buffet, P. A., Dao, M., & Suresh, S. (2016). Biomechanics of red blood cells in human spleen and consequences for physiology and disease. *Proceedings of the National Academy of Sciences of the United States of America*, *113*, 7804–7809.

Reinhart, W. H., & Chien, S. (1985). Roles of cell geometry and cellular viscosity in red cell passage through narrow pores. *The American Journal of Physiology*, *248*, C473–C479.

Renia, L., Howland, S. W., Claser, C., Gruner, A.C., Suwanarusk, R., Hui Teo, T., … Ng, L. F. (2012). Cerebral malaria: Mysteries at the blood-brain barrier. *Virulence*, *3*, 193–201.

Renoux, C., Faivre, M., Bessaa, A., Da Costa, L., Joly, P., Gauthier, A., & Connes, P. (2019). Impact of surface-area-to-volume ratio, internal viscosity and membrane viscoelasticity on red blood cell deformability measured in isotonic condition. *Scientific Reports*, *9*, 6771.

Safeukui, I., Buffet, P. A., Deplaine, G., Perrot, S., Brousse, V., Ndour, A., … Mohandas, N. (2012). Quantitative assessment of sensing and sequestration of spherocytic erythrocytes by the human spleen. *Blood*, *120*, 424–430.

Safeukui, I., Buffet, P. A., Deplaine, G., Perrot, S., Brousse, V., Sauvanet, A., … Mohandas, N. (2018). Sensing of red blood cells with decreased membrane deformability by the human spleen. *Blood Advances*, *2*, 2581–2587.

Schilling, R. F., Gangnon, R. E., & Traver, M. I. (2008). Delayed adverse vascular events after splenectomy in hereditary spherocytosis. *Journal of Thrombosis and Haemostasis*, *6*, 1289–1295.

Shin, S., Ku, Y., Park, M.-S., & Suh, J.-S. (2005). Slit-flow ektacytometry: Laser diffraction in a slit rheometer. *Cytometry Part B: Clinical Cytometry*, *65B*, 6–13.

Singh, B., & Daneshvar, C. (2013). Human infections and detection of *Plasmodium knowlesi*. *Clinical Microbiology Reviews*, *26*, 165–184.

Sosa, J. M., Nielsen, N. D., Vignes, S. M., Chen, T. G., & Shevkoplyas, S. S. (2014). The relationship between red blood cell deformability metrics and perfusion of an artificial microvascular network. *Clinical Hemorheology and Microcirculation*, *57*, 275–289.

Suresh, S., Spatz, J., Mills, J. P., Micoulet, A., Dao, M., Lim, C. T., … Seufferlein, T. (2005). Connections between single-cell biomechanics and human disease states: Gastrointestinal cancer and malaria. *Acta Biomaterialia*, *1*, 15–30.

Suzuki, Y., Tateishi, N., Soutani, M., & Maeda, N. (1996). Flow behavior of erythrocytes in microvessels and glass capillaries: Effects of erythrocyte deformation and erythrocyte aggregation. *International Journal of Microcirculation, Clinical and Experimental*, *16*, 187–194.

Tomaiuolo, G. (2014). Biomechanical properties of red blood cells in health and disease towards microfluidics. *Biomicrofluidics*, *8*, 051501.

Van Avondt, K., Nur, E., & Zeerleder, S. (2019). Mechanisms of haemolysis-induced kidney injury. *Nature Reviews. Nephrology*, *15*, 671–692.

Wahlgren, M., Goel, S., & Akhouri, R. R. (2017). Variant surface antigens of *Plasmodium falciparum* and their roles in severe malaria. *Nature Reviews. Microbiology*, *15*, 479–491.

Waldecker, M., Dasanna, A. K., Lansche, C., Linke, M., Srismith, S., Cyrklaff, M., … Lanzer, M. (2017). Differential time-dependent volumetric and surface area changes and delayed induction of new permeation pathways in *P. falciparum*-infected hemoglobinopathic erythrocytes. *Cell Microbiology*, *19*(2), e12650.

Warkentin, T. E., Barr, R. D., Ali, M. A., & Mohandas, N. (1990). Recurrent acute splenic sequestration crisis due to interacting genetic defects: Hemoglobin SC disease and hereditary spherocytosis. *Blood*, *75*, 266–270.

Warrell, D. A., White, N. J., Veall, N., Looareesuwan, S., Chanthavanich, P., Phillips, R. E., … Krishna, S. (1988). Cerebral anaerobic glycolysis and reduced cerebral oxygen transport in human cerebral malaria. *Lancet*, *2*, 534–538.

Waugh, R. E., McKenney, J. B., Bauserman, R. G., Brooks, D. M., Valeri, C. R., & Snyder, L. M. (1997). Surface area and volume changes during maturation of reticulocytes in the circulation of the baboon. *The Journal of Laboratory and Clinical Medicine*, *129*, 527–535.

Xie, J., Zhou, J., & Fung, Y. C. (1995). Bending of blood vessel wall: Stress-strain laws of the intima-media and adventitial layers. *Journal of Biomechanical Engineering*, *117*, 136–145.

Yeoh, O. H. (1990). Characterization of elastic properties of carbon-black-filled rubber vulcanizates. *Rubber Chemistry and Technology*, *63*, 792–805.

Yoon, D., & You, D. (2016). Continuum modeling of deformation and aggregation of red blood cells. *Journal of Biomechanics*, *49*, 2267–2279.

Zhang, Y., Huang, C., Kim, S., Golkaram, M., Dixon, M. W., Tilley, L., … Suresh, S. (2015). Multiple stiffening effects of nanoscale knobs on human red blood cells infected with *Plasmodium falciparum* malaria parasite. *Proceedings of the National Academy of Sciences of the United States of America*, *112*, 6068–6073.

## SUPPORTING INFORMATION

Additional supporting information may be found online in the Supporting Information section at the end of this article.

**How to cite this article:** Namvar A, Blanch AJ, Dixon MW, et al. Surface area-to-volume ratio, not cellular viscoelasticity, is the major determinant of red blood cell traversal through small channels. *Cellular Microbiology*. 2020;e13270. https://doi.org/10.1111/cmi.13270